Proc Indian Natn Sci Acad, **70, A,** No. 2, March 2004, pp. 267-281

ELECTRON TRANSFER SITES IN BIOINORGANIC CHEMISTRY

EDWARD I SOLOMON*, LIPIKA BASUMALLICK,
ABHISHEK DEY AND RITIMUKTA SARANGI

Stanford University, Stanford, California-94305 (USA)

(Received 20 November 2002 ; Accepted 27 November 2002)

Metalloprotein active sites exhibit unique spectroscopic features, which reflect novel electronic structures that can make major contributions to biological function. In this review we consider the blue copper, Cu_A and FeS centres involved in biological electron transfer. For blue copper, we consider the high anisotropic covalency of the thiolate-Cu(II) bond, its contribution to ET and the effects of variation in axial and equatorial ligands on this bond. For Cu_A, we consider the origin of electron delocalization in the mixed-valent site, the associated ground state wave function and their contributions to rapid long range electron transfer. Finally, for the FeS centres we introduce sulfur K-edge spectroscopy as a direct experimental probe of ligand metal covalency and use this to define differences in μ_2 vs. μ_3 sulfide covalency, which relates to the difference in localization in mixed-valent Fe_2S_2 centres vs. delocalization in Fe_4S_4 sites. Finally, this method allows a direct probe of protein derived H-bonding effects on the electronic structures of the iron sulfur active sites.

Key Words : Metalloprotein; Electron Transfer; Blue Copper; Cu_A; Mixed-Valent Compounds; Iron-Sulfur sites, Ligand K-edge Spectroscopy

1 Introduction

Metalloproteins play key roles in biological electron transfer. They are involved in a number of important biological functions including respiratory metabolism, photosynthesis and nitrogen fixation where they mediate inter-protein[1] or intra-protein[2] electron transfer[3]. The electron transfer metalloproteins can be broadly classified as having heme containing and non-heme active sites.

The most common heme containing electron transfer sites are cytochrome *b* and *c*. The site in cytochrome *b* has a non-covalently bound protoporphyrin, while cytochrome *c* has the heme prosthetic group covalently bound to the protein through thioether linkages. The cytochromes have varying axial ligands, the most common being two histidines in cytochrome *b* and a histidine and a methionine in cytochrome *c*[4]. The properties of these heme centres are dominated by intense porphyrin $\pi \rightarrow \pi^*$ transitions and iron-porphyrin charge transfer transitions. Good reviews exist for heme electron transfer sites[5-10]. Here, we will focus on the geometric and electronic structure of copper and iron-sulfur electron transfer sites.

The active sites of some of the non-heme electron transfer proteins are summarized in Fig. 1. The electron transfer active sites generally exhibit unique spectral features, which reflect novel electronic structures that make significant contributions to reactivity[11,12]. The blue copper centre found in plastocyanin (Fig. 1a), azurin and related proteins have a Cu ion in a trigonally distorted tetrahedral geometry[13-15]. The equatorial ligand set includes a cysteine with an unusually short Cu-S(Cys) bond (~2.1 Å) and two histidines with typical Cu-N(His) bonds (~2.0 Å). The axial ligand is usually a methionine with a long ~2.9 Å Cu-S(Met) bond[16]. The unique spectral features include an intense absorption band at ~600 nm (ε ~5000 $M^{-1}cm^{-1}$)[12,17] and a small $A_{\|}$ value in the EPR spectrum (<100 x 10^{-4} cm^{-1})[18] indicating high covalency of the Cu-S(Cys) π bond (*vide infra*). There are also a number of 'perturbed' blue copper sites, which exhibit substantially different spectral features[19-24] than those of classical blue sites. They either exhibit shorter axial Cu-S(Met) bond (*e.g.* nitrite reductase, cucumber basic protein) or have the axial ligand substituted (*e.g.* stellacyanin, fungal laccases). Blue copper centres are characterized by high reduction potentials (180-780 mV) compared to that of normal copper complexes (~150 mV) and are suited for rapid long-range electron transfer.

The Cu_A site (Fig. 1b) found in cytochrome *c* oxidase[25] and nitrous oxide reductase is binuclear with the two coppers separated by ~2.4 Å[26,27] and bridged by two cysteines forming a planar 'diamond core'[28-31]. The copper sites are trigonal with the third ligand being an equatorial histidine. The axial ligand on one copper

*Author for correspondence *e-mail* : Edward.Solomon@stanford.edu
fax: (650) 725-0259

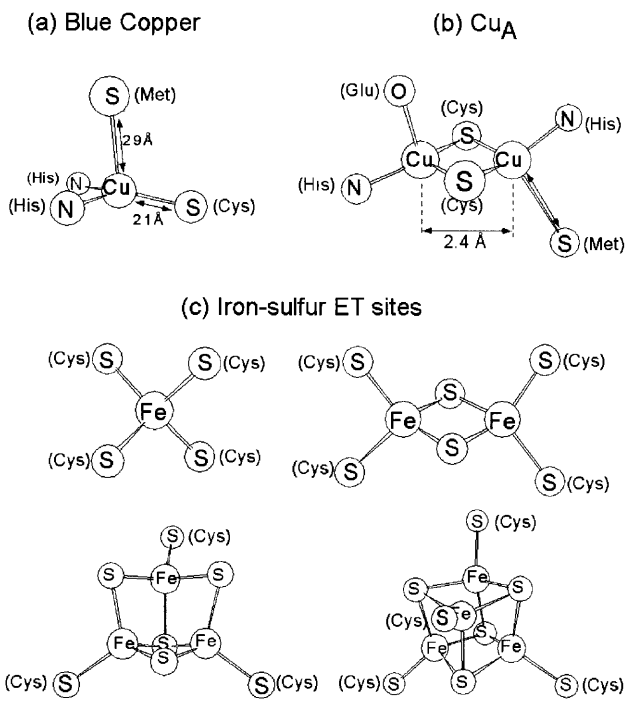

Fig. 1 Cu and Fe-S electron transfer centres. (a) blue copper centre (b) Cu_A centre (c) mononuclear rubredoxin, binuclear [2Fe-2S] ferredoxin, trinuclear [3Fe-4S] ferredoxin and tetranuclear [4Fe-4S] ferredoxin (HiPIP)

is a methionine and on the other is a backbone carbonyl oxygen. The Cu_A centre has an EPR signal exhibiting seven hyperfine split resonances at $g_{\|}$ (consistent with a class III delocalized dimer of I = 3/2 Cu nuclei)[32], a low $g_{\|}$ value and intense absorption bands at 750 nm and two bands centered at 500 nm, the former being the $\psi \rightarrow \psi^*$ transition of the Cu-Cu bond and the later the bridging S(Cys)→Cu charge transfer transitions. The interesting feature for this site is the presence a Cu-Cu bond and its complete delocalization even in the low-symmetry protein environment[33,34].

The common iron sulfur centres (Fig. 1c) have either one iron with four cysteine ligands in a distorted tetrahedral environment (rubredoxin), or two, three, or four iron clusters (the list includes ferredoxins and the high potential iron proteins) with μ_2 and μ_3 sulfide bridges[25,35-37]. Iron sulfur clusters from different organisms show variation in Fe-S bond lengths (2.2 Å to 2.4 Å). The distance between two iron centres is 2.7 Å in both dimers and tetramers. The iron sulfur centres have intense charge transfer absorption features due to sulfur ligation and EPR properties which in the monomer reflects a highly covalent Fe-thiolate bonding interaction, and in the clusters exhibit interactions between the irons due to antiferromagnetic coupling and double exchange. In the two iron mixed valent reduced cluster ($Fe^{II}Fe^{III}$) the iron centres are localized and antiferromagnetically coupled [38,39], while in the three and four iron clusters the reduced two iron sub-site is delocalized and ferromagnetically coupled *via* a double exchange mechanism[40,41].

In considering the reactivity of these metalloprotein active sites, one focuses on contributions from both the thermodynamic (*i.e.* reduction potential) and the kinetic (k_{ET}) properties of electron transfer. The reduction potential is affected by the ionization energy of the active site, which is influenced by the effective nuclear charge on the metal, the energy of the redox active orbital and electronic relaxation. There is also a large environment term due to differential solvent stabilization of the different redox states (Born equation: the free energy change for transferring an ion from a dielectric constant of ε^1 to one of ε^2 is $\Delta G = 166q^2/r * (1/\varepsilon^2 - 1/\varepsilon^1)$ where q is the charge and r is its radius) as well as contributions from dipole moments and H bonds[3,42]. The kinetics of electron transfer reactions are described by the semi-classical Marcus[43] equation $k_{ET} = v\pi/(\hbar^2 \lambda k_B T).(H_{DA})^2.exp[-(\Delta G^{\dagger}+\lambda)^2/(4\lambda k_B T)]$ which shows the rate of electron transfer is dependent on the difference in the reduction potential of the donor and the acceptor ($\Delta G^{\dagger}$); the electronic coupling through the protein (H_{DA}) and the reorganization energy associated with the active site geometry (λ_{inner}) and the reorientation of the solvent dipoles (λ_{outer}). In this review, we will focus on how the electronic structure of active sites influence the important thermodynamic and kinetic parameters of electron transfer.

2 Mononuclear Copper Electron Transfer Centres

2.1 Classic Blue Copper

The oxidized prototypical blue copper protein (*e.g.* plastocyanin) exhibits an intense S(Cys)→Cu charge transfer absorption band in the 600 nm region ($\varepsilon \sim 5000\ M^{-1}cm^{-1}$, Fig. 2a), resulting in its pronounced blue colour [12]. The electron paramagnetic resonance Cu hyperfine splitting ($<70 \times 10^{-4}\ cm^{-1}$) is reduced to less than half the value observed for normal Cu(II) complexes ($150 \times 10^{-4}\ cm^{-1}$, Fig. 2b) [18]. These unique spectral features have been attributed to the highly covalent Cu-S(Cys) interaction. The sulfur covalency has been directly determined by the S-K edge X-ray absorption spectroscopy[44] where the intensity of the S-K pre-edge feature reflects the amount of S(Cys) 3p character in the half occupied Cu $3d_{x^2-y^2}$ orbital[45]

(38% in plastocyanin). The complementary Cu L-edge X-ray absorption spectroscopy experiment evaluates the Cu d-character in the HOMO (42% in plastocyanin versus 60-70% in normal tetragonal Cu complexes)[46] through the analysis of the Cu 2p→3d transition intensity. The highly covalent bonding interaction between Cu and the S(Cys) contributes significantly to the electronic coupling matrix element (H_{DA}) for long-range electron transfer through the cysteine.

Studies of the reduced blue copper site have shown that the long thioether S(Met)-Cu^{1+} bond is imposed on the active site by the protein[47]. The reduced thioether donation to the Cu due to a long S(Met)-Cu bond is compensated by the short, strong Cu-thiolate bond. Together these eliminate the Jahn-Teller distorting force upon going to the oxidized state by removing electronic degeneracy of the d_{xy} and $d_{x^2-y^2}$ orbitals (experimentally observed to be split by 10800 cm^{-1} in the low temperature MCD spectrum)[48]. This leads to very little geometry change with oxidation and hence a low reorganization energy (λ_{inner}). The electronic structure of the blue copper site is thus favourable for rapid long-range electron transfer.

2.2 *Perturbed Blue Copper*

2.2.1 Role of Axial Ligand

Axial perturbations of the classical blue copper site could be divided into two classes. In one class, the axial methionine is replaced either by a stronger field ligand (*e.g.* glutamine in stellacyanin) or is replaced with a non-ligating group (*e.g.* leucine or phenylalanine in fungal laccases) and hence no axial ligand is present. The second class has the same ligand set as plastocyanin and azurin yet exhibits dramatic spectral differences,

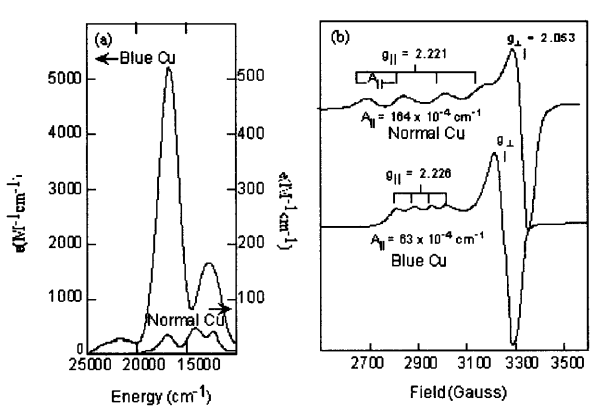

Fig. 2 Low temperature UV/Vis absorption (a) and electron paramagnetic resonance spectra (b) of poplar plastocyanin (blue Cu centre) vs. normal tetragonal copper complex.

including a colour change of the oxidized site from blue to green, over the series: plastocyanin (blue) → cucumber basic protein → nitrite reductase (green). In this review we will focus on the second group of perturbed sites[24].

The type I copper site in nitrite reductase from *Achromobacter cycloclastes* is characterized by increased absorption intensity at 450 nm and a corresponding decrease in the intensity of the 600 nm band [24], which leads to its green colour (Fig. 3a). The spectral changes corresponding to a decrease in the S(Cys) π and an increase in the S(Cys) σ to Cu $3d_{x^2-y^2}$ charge transfer intensities, respectively, indicate that the half occupied $3d_{x^2-y^2}$ orbital is rotated from π to σ bonding interaction with the thiolate ligand in green relative to the blue site [24]. In addition, its low temperature MCD (Fig. 3b) indicates that the ligand field transitions have shifted to higher energy relative to plastocyanin. The crystal structure [13,16] shows that on going from plastocyanin to nitrite reductase, the axial Cu-S(Met) bond length decreases by ~0.3 Å, the equatorial Cu-S(Cys) bond increases by >0.1 Å and the S(Cys)-Cu-S(Met) plane rotates relative to the N(His)-Cu-N(His) plane. This leads to more tetragonal ligand geometry in the green relative to the blue site and thus a stronger ligand field as observed in the MCD ligand field transition energies in Fig. 3b. The weakened thiolate-Cu interaction due to a longer Cu-S(Cys) bond in the green site is consistent with the decreased Cu-S(Cys) stretching frequency ($\langle\nu_{Cu\text{-}S}\rangle$ = 383 cm^{-1} in nitrite reductase *vs.* 403 cm^{-1} in plastocyanin) in the resonance Raman spectrum[49]. This has lead to the coupled distortion model (Fig. 3c) where the stronger axial S(Met)-Cu interaction due to the shorter Cu-S(Met) bond is coupled with the weakened S(Cys)-Cu bond and together result in the tetragonal distortion of the ligand field and rotation of the Cu $3d_{x^2-y^2}$ from π to σ bonding to the S(Cys). The reduction potential along the series decreases from ~370 mV in plastocyanin to ~240 mV in nitrite reductase. This is consistent with the increased tetragonal (Jahn-Teller type) distortion and stronger thioether donor interaction lowering the energy (*i.e.* stabilizing) the oxidized site at the green site in nitrite reductase compared to the classic site in plastocyanin[24].

2.2.2 Effect of Increased Ligation at the Copper Centre

A number of blue copper related sites have five ligands (*e.g.* the red copper protein, nitrosocyanin)[50,51]

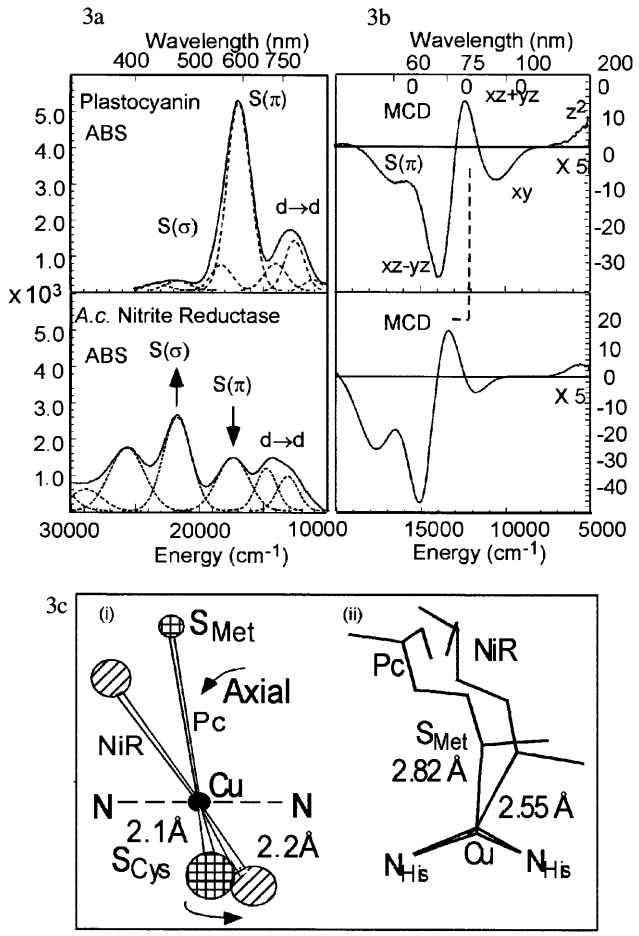

Fig. 3 Classic and perturbed blue copper sites : (a) Low temperature absorption (left) showing redistribution of spectral intensity in S(Cys) → Cu π and σ charge transfer bands. Magnetic circular dichroism spectra (right) showing the shift of ligand field transitions to higher energy, (b) The tetragonal Jahn-Teller distortion, (c) Crystal structures showing contraction of S(Met)-Cu bond and the elongation of the S(Cys)-Cu bond

rather than the four ligands present in the classic blue copper sites such as plastocyanin and azurin. The effect of this increased ligation has been investigated in inorganic model complexes: the 5-coordinate $[Cu(SMeIm)(HB(3,5\text{-}iPr_2pz)_3)]$[52-54] complex and the 4-coordinate $[Cu(SCPh_3)(HB(3,5\text{-}iPr_2pz)_3)]$[52-55] complex, which mimic the structural and spectroscopic features of the active sites of red and blue copper centres, respectively. The key spectral differences in the low temperature absorption and magnetic circular dichroism spectra of the 5-coordinate complex (Fig. 4a)[56] include an increase in the S σ→Cu charge transfer band (370 nm) intensity and a decrease in the S π→Cu charge transfer transition (570 nm) intensity compared to the 4-coordinate complex. The d→d transitions shift up in energy as observed in the MCD spectra in the 5-coordinate relative to the 4-coordinate reflecting a more tetragonal geometry and a stronger ligand field in the 5-coordinate complex. S K-edge X-ray absorption spectroscopy (XAS) measurements demonstrate a less covalent Cu-thiolate interaction in the 5-coordinate (15% S p in the HOMO) relative to the 4-coordinate (52% S p). Cu L-edge XAS indicates the Cu d-character in the HOMO of the 5-coordinate has increased (45%) relative to that of the 4-coordinate complex (36%). These spectral features result from the shift of the thiolate ligand position in the NNS plane with an increased equatorial coordination and thus an increased σ overlap between the S p and the Cu $3d_{x^2-y^2}$ orbital in the 5-coordinate complex[56]. Additionally, there is an increase in the Cu-S bond length in the 5-coordinate (2.45 Å) compared to the 4-coordinate (2.13 Å) complex. These geometric perturbations in the 5-coordinate site, due to the increased ligation, lead to a reduced covalency of the thiolate-Cu bond and the rotation of the thiolate to have a dominant σ interaction with the Cu centre and should significantly impact the reactivity for these ET sites (Fig. 4b).

3 Binuclear Copper Electron Transfer Active Sites

The binuclear Cu_A centre present in cytochrome *c* oxidase (C*c*O) and nitrous oxide reductase [25,57,58] is an important inter- and intra-molecular electron transfer active site. In the oxidized form, Cu_A centre is a completely delocalized (class III) mixed valent binuclear centre with two $Cu^{1.5+}$ atoms separated by ~2.44 Å [59,60] and bridged by two S(Cys) to form a Cu_2S_2 diamond core structure (Fig. 5a). The Cu centres are trigonal, with an N(His) providing the third equatorial ligand. The axial ligand on one Cu is an S(Met) and that on the other is carbonyl oxygen of Gln coming from a polypeptide backbone in the protein. Early EPR studies resulted in seven hyperfine lines suggesting identical copper atoms (Fig. 6), which was surprising given the difference in ligand environment (Fig. 5a) and indicated complete delocalization of the Cu centres. An intense S(Cys)→Cu $3d_{x^2-y^2}$ charge-transfer (CT) was observed (Fig. 7 top solid line) reflecting high anisotropic covalency of the Cu-thiolate bond, similar to that observed in blue copper proteins which are also involved in inter-and intra-molecular ET. Parallel spectroscopic studies were also performed on a mixed-valence (MV) model system (Fig. 5b)[61], which give useful insight into the unique nature of Cu_A system. In

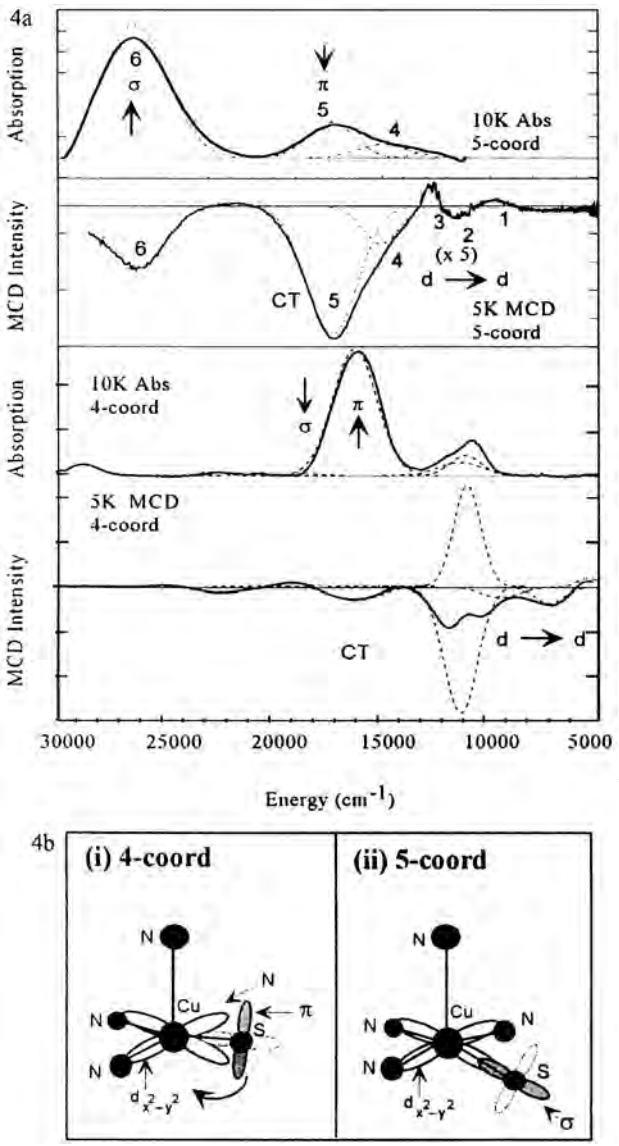

Fig. 4 (a) Electronic spectra of the five coordinate complex [Cu(SMeIm)(HB(3,5-iPr$_2$pz)$_3$)] in comparison to the four coordinate complex [Cu(SCPh$_3$)(HB(3,5-iPr$_2$pz)$_3$)]. Low temperature absorption at 10 K. Magnetic circular dichroism at 5 K and 7 T, (b) Cu- S(thiolate) bonding interactions: four coordinate illustrates the strong π-weak σ, while the five coordinate depicts the strong σ-weak π interaction.

this review we focus on the characterization of the unique spectral features observed for the engineered Cu_A azurin construct, determination of the origin of complete delocalization in the low symmetry site and the correlation of these observations with the redox and ET properties of Cu_A.

3.1 Electron Delocalization Pathway

In a mixed-valent bridged binuclear metal centre such as Cu_A, electronic delocalization and metal-metal interaction can occur mainly through two pathways, an indirect ligand based superexchange pathway and a direct metal-metal overlap. A quantitative estimate of the Cu-Cu interaction or the electron coupling matrix element ($2H_{Cu-Cu}$) was obtained from the $\psi \rightarrow \psi^*$ transition energy, where ψ and ψ^* are the bonding and the singly occupied antibonding orbital (HOMO) for the binuclear centre, respectively. In the MV model (Fig. 5b) the two Cu centres are also linked by two thiolate bridges and are completely delocalized. The Cu-Cu distance in the MV model is ~2.9 Å, which does not allow direct δ-type Cu-Cu overlap. Band assignments of the absorption and MCD spectra in Fig. 7 revealed that the Cu-Cu $\psi \rightarrow \psi^*$ in the MV model (band 1) appears at ~5560 cm^{-1} while in Cu_A the $\psi \rightarrow \psi^*$ transition occurs at ~13400 cm^{-1} [33,55,62] (band 3). Since the % S covalency from sulfur K-Edge for Cu_A and the MV model are similar (*vide infra*), the contribution to $2H_{Cu-Cu}$ from the superexchange pathway, which is proportional to the Cu-S overlap, is comparable. The significant change in the $\psi \rightarrow \psi^*$ transition energy must be attributed to the presence of a direct Cu-Cu overlap which is feasible at a separation of ~2.4 Å. Thus the direct Cu-Cu interaction contributes 7800 cm^{-1} to $2H_{Cu-Cu}$.or ~60% to the total electronic configuration functional delocalization. A second apparent difference is observed between the absorption spectra of Cu_A and the MV model (in Fig. 7 top), namely the energy shift of the intense charge transfer peak due to S(Cys)→Cu transition from 28000 cm^{-1} in the MV model to 20000 cm^{-1} in Cu_A [33]. This shift is similar to that observed between blue copper proteins and the corresponding monothiolate models indicating a weakened axial bonding interactions in Cu_A [63].

3.2 Ground State Wave Function of Cu_A

A quantitative description of the ground state (GS) wave function for Cu_A and the MV model has been elucidated by using S K-edge and Cu L-edge X-ray absorption spectroscopies combined with DFT calculations. The GS wave function of the singly occupied HOMO is approximately given by:

$$\Psi_{HOMO} \approx [1-\alpha^2-\beta^2]^{1/2} |Cu\ 3d\rangle - \alpha |S\ 3p\rangle - \beta |other(Ligands)\rangle$$

S K-edge XAS probes the Sulfur 1s→3p electric dipole allowed transition (see section 4 for details). The Cu-S covalency, α^2, is obtained from the pre-edge intensity in the spectrum (Fig. 8b)[34], which describes the amount of S 3p in the Ψ_{HOMO}. The β^2 term in the HOMO corresponds to the mixing of other ligand orbitals with Cu 3d orbital. Cu L-edge XAS

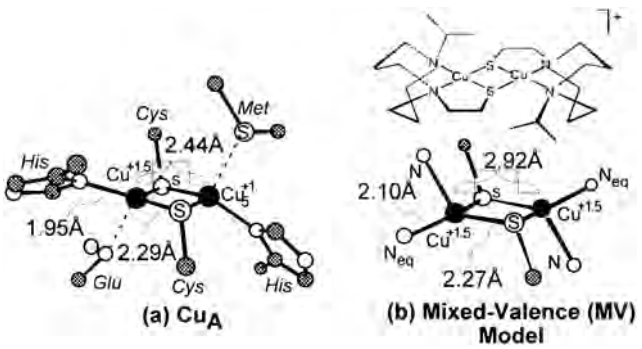

Fig. 5 (a) The Cu centre in cytochrome c oxidase, (b) the mixed-valence model complex.

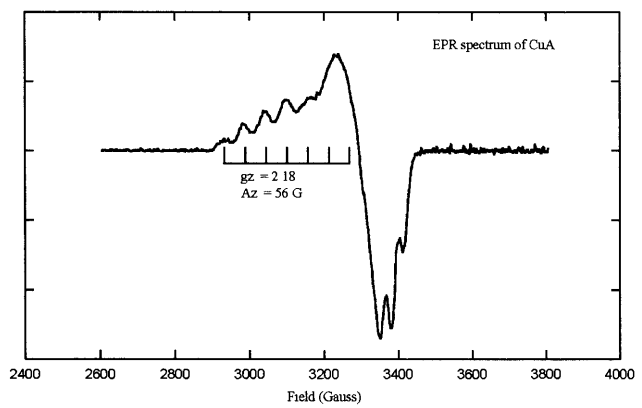

Fig. 6 The X-band EPR spectrum of the engineered Cu_A azurin construct. T = 77 K.

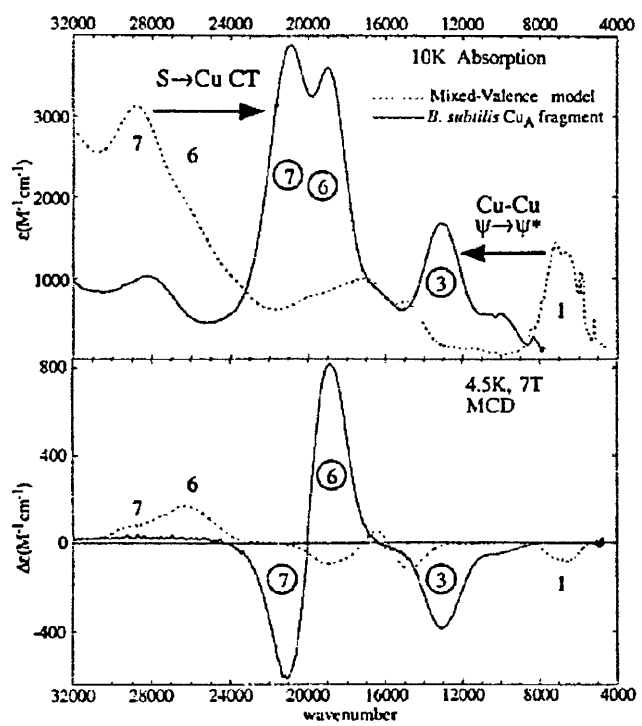

Fig. 7 Low temperature absorption and MCD spectra of Cu_A and the mixed-valent model.

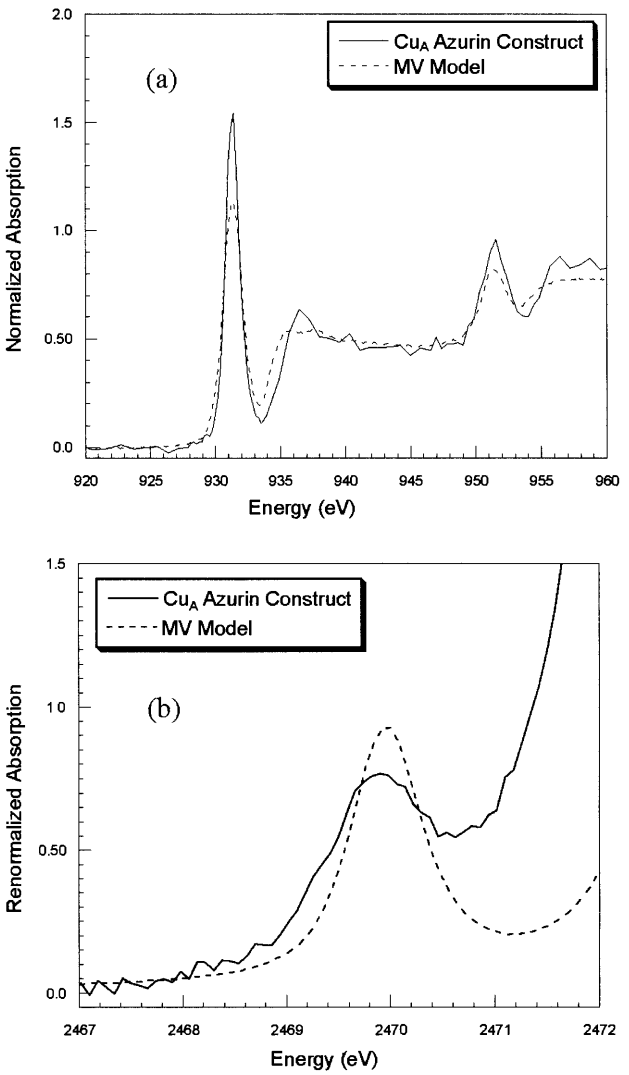

Fig. 8 (a) Comparison of the normalized Cu L-edge spectra of Cu (from engineered azurin construct) and the mixed valent model, (b) A comparative S K-edge spectra of CuA (from engineered azurin construct) and the mixed valent model.

quantitatively probes the dipole allowed Cu 2p →3d transition. The combined intensity observed under the L_3 and L_2 peaks, gives the total 3d orbital covalency $(1-\alpha^2-\beta^2)$ in the singly occupied Ψ_{HOMO}. These experimental techniques together give a quantitative description of the ground state wave function. The normalized S covalency obtained for the Cu_A azurin construct is 46 ± 2% while that obtained for the MV model is 54 ± 2.5% (Fig. 8b). The S 1s energies, which are largely dependent on charge donation are assumed to be similar due to similar Cu-S covalencies. The pre-edge transition energy in Cu_A and the MV model appear respectively at 2469.9 and 2470.0 eV (Fig. 8b) indicating that the HOMO on Cu is at very similar

energies in both molecules. The ligand field of Cu_A has been shown to be ~0.4 eV less than the MV model by spectroscopy and calculations. In addition[33], a lower Z_{eff} in the MV model should shift its spectrum to higher energies. The combined effect of Z_{eff} and ligand field is countered by the metal-metal bond, which accounts for ~0.4 eV shift to higher energies in Cu_A. Cu L-edge XAS studies of the two complexes (Fig. 8a) give 44 ± 1% and 38 ± 0.4% total copper character in the HOMO of Cu_A and the MV model respectively [34]. The similar L_3 and L_2 pre-edge energy peak positions indicate that in Cu_A the interplay of the decreasing effect of Z_{eff} and the increasing effect of metal-metal bond cancel giving a similar situation as the S K-edge. Thus the L_3 and L_2 peaks for Cu_A appear at 931.4 eV and 951.5 eV respectively and at 931.3 eV and 951.4 eV for the MV model. In addition, from[14,15] N-ENDOR[64,65] and ^{1}H-ENDOR[64] studies performed on Cu_A the N(His) and β-methylene H atoms of cysteine residue contribute 6% and 3% to the covalency. The experimentally observed covalencies (Cu d +S p +N total +H total) contribute a total of ~99 ± 7% to the HOMO. Furthermore, an MO analysis of Cu_A and the MV model based on spectroscopy reveals that the HOMO on Cu in the MV model is π type with mainly Cu $3d_{xy}$ character, while that on Cu_A is σ type with Cu $3d_{x^2-y^2}$ character, this can be viewed as a rotation of the Ψ^*_{HOMO} (Fig. 9). This rotation of the ground state Ψ^*_{HOMO} keeps the Cu_2S_2 core delocalized by facilitating a Cu-Cu bond in Cu_A unlike in the MV model where the only contribution to delocalization is by a ligand based superexchange pathway.

3.3 Structure Function Correlation

The binuclear Cu_A centre performs both inter- and intra-molecular electron transfer in C*c*O and nitrous oxide reductase. The rate of ET is dependent on the three parameters in the Marcus equation[43,66], the donor-acceptor electronic coupling (H_{DA}), the Franck-Condon reorganization energy associated with the ET and the difference in redox potential (ΔG°). In Cu_A the high anisotropic covalency of the Cu-S(Cys) bond (i.e., H_{DA}) significantly enhances the Cu_A input ET rate. A pathways calculation reveals that a highly covalent Cu-S(Cys) bond makes ET pathways *via* Cu-S(Cys196) and Cu-S(Cys200) competitive with the Cu-N(His204) pathway (Fig. 10). Pathways calculations on the ET input pathway from cytochrome c to the surface of C*c*O and into Cu_A *via* Trp104, which is a key residue in the ET pathway, have also been performed. Inclusion of the anisotropic covalency of Cu-S (Cys 200) into the calculations give a rate of 5.1 x 10^4 s^{-1} which is consistent with experiment[34]. A reorganization energy of only 2000 cm^{-1} in Cu_A is attributed to its dimeric nature, where the distribution of nuclear reorganization over a dimer reduces both the inner and outer sphere reorganization energies by a factor of ~2. The redox potential of oxidized Cu_A is ~+250 mV which is within the range observed for blue copper proteins. In Cu_A, the short Cu-S(Cys) tends to stabilize the higher oxidation state by electron donation into copper while long axial interaction tends to destabilize the copper towards Cu(I). The two strong in plane Cu-S bonds should drive the reduction potential to a value much lower than +250 mV[67], however, the presence of a Cu-Cu bond raises the redox potential through delocalization to the second copper centre to a value relevant to ET. The valence delocalization may be biologically designed to tune the redox potential and to

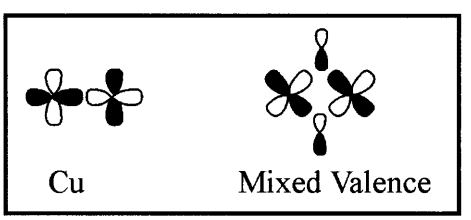

Fig. 9 Molecular orbital showing bonding scheme in the Cu_A centre and the mixed-valent model complex.

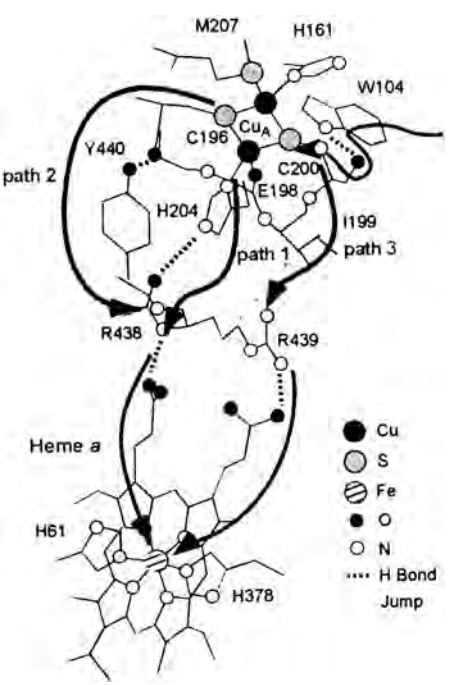

Fig. 10 Proposed ET pathways in bovine heart cytochrome c oxidase.

facilitate ET through different pathways. Thus, delocalization in a low symmetry protein site, resulting from Cu-Cu bonding plays a major role in the ET properties of Cu_A.

4 Fe-S Electron Transfer Centres

4.1 Ligand K-edge X-ray Absorption Spectroscopy (XAS) - A direct probe of Metal-Ligand Covalency

The K-edge XAS of a ligand has proven to be a powerful method in estimating metal ligand covalency. The electric dipole allowed transitions for K-edges are ligand 1s $\rightarrow$ np transitions. Ligand K-edge XAS of d^9 Cu(II) complexes show a well defined pre-edge feature which was assigned to the transition from ligand 1s orbital to the half occupied Highest Occupied Molecular Orbital (HOMO) of Cu(II), ψ^*[44,68]. Due to the localized nature of the ligand (L) 1s orbital this transition can have intensity only if the HOMO contains significant ligand np character due to covalency

$$\psi^* = (1-\alpha^2)^{1/2} |M\ 3d> - \alpha| Lnp> \quad ...(1)$$

The intensity of the transition from any ligand L to the Cu ψ^* is

$$\boldsymbol{I}\ (L1s\rightarrow \psi^*) = \text{const}\ |\langle L_{1s}|\mathbf{r}|\psi^*\rangle|^2 \quad ...(2)$$

which can be rewritten as

$$= \alpha^2.\text{const.}\ |\langle L_{1s}|\mathbf{r}|L_{np}\rangle|^2 \quad ...(3)$$

$$= \alpha^2.\ \mathbf{I}(1s\rightarrow np)$$

where $\mathbf{I}(1s\rightarrow np)$ is the intensity of a pure electric dipole allowed ligand 1s$\rightarrow$np transition.

Thus, the pre-edge intensity provides a quantitative estimate of the ligand contribution to the HOMO due to bonding. The pre-edge XAS intensity for metal centres with d^n configurations also corresponds to the amount of ligand np character summed over the metal d antibonding orbitals[69,70].

A direct relation between the ligand K-edge XAS intensity (D_o) and covalency (α^2) of the unoccupied metal holes is given by[71]

$$\text{Covalency}^2 = D_o/\text{constant} \quad ...(4)$$

Transition moment integrals for individual ligands are found by using previously determined covalency and the experimental D_o from XAS. The thiolate covalency of Cu-S cysteine bond of the active site of plastocyanin was determined to be 38%[45] which corresponds to a experimental D_o of 1.02. Using this, the transition dipole integral was found to be 8.05. Correspondingly the transition dipole integral for a μ_2 bridging sulfide was estimated to be 6.54 by comparing the experimental D_o of the infinite chain $CsFeS_2$ complex to the measured covalency from XPS experiments[72]. Calculations show[72] that the dependence of the transition moment integral $\langle L_{1s}|\mathbf{r}|L_{3p}\rangle$ on effective nuclear charge is linear over the range that the effective nuclear charge is expected to change in transition metal complexes.

Generally, the analysis of the metal K-edge XAS spectra are complicated by final state relaxation due to the core hole created upon the excitation. The relaxation gives rise to formally forbidden two electron transitions called the shake-up transitions. These involve the creation of a new hole and a MLCT to neutralize this positive hole formed. In case of ligand K-edges these are generally not observed. This is because ligands such as Cl^- are π donor ligands do not have low-lying acceptor orbitals and a MLCT is not expected. This is further supported by molecular orbital calculations [69].

4.2 Ground State Electronic Structure Determination of Fe-S Active Sites Using XAS

4.2.1 Electronic Structure of Monomeric Fe-S_4 Clusters in Rubredoxins

Rubredoxins are small globular metalloproteins that function as an electron transport agent in biology. It is the simplest among the Fe-S sites in terms of electronic structure and it has one iron coordinated by four sulfur from cysteine residues in a distorted tetrahedral geometry (Fig. 1). The biologically relevant reaction of these proteins involves a one electron Fe(III)/Fe(II) couple. The Fe-S bonds were known to be very covalent and hence the tuning of this covalency can be instrumental in modifying the electronic properties of these active sites.

S-K edge XAS of some model complexes are shown[70] in Fig. 11. In case of Fe(II) the pre-edge feature shifts to a higher energy and overlaps with the rising edge structure. The energy shift here is primarily due to reduction of effective nuclear charge of the metal when one more electron is added. The covalency of oxidized and reduced $Fe(II)(SPh)_4$ shows that there is a large decrease in total covalency from 154% to 84% on reduction implying that some charge density is delocalized in to ligands on reduction. This correlates nicely to the huge relaxation seen in these sites on reduction[73].

4.2.2 Electronic Structure of Dimeric [Fe_2S_2] Cluster in Model Compounds with Relevance to Protein Sites

S K-edge XAS was particularly insightful in the case of the dimeric and the tetrameric [Fe_n-S_n] centres. The dimeric [Fe_2S_2] centre has two μ_2 bridging sulfides

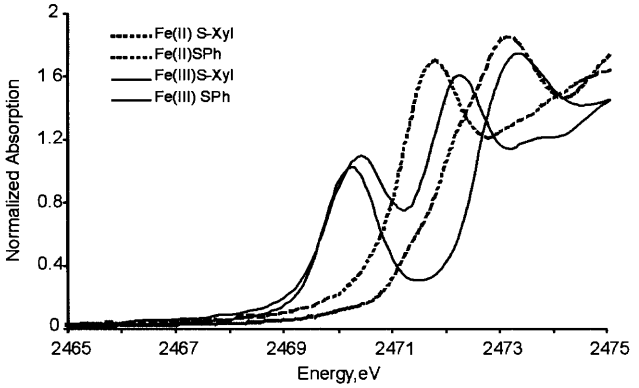

Fig. 11 XAS spectra of rubredoxin model complexes $[Fe(S_2\text{-}Xyl)_2]^{-1}$, $[Fe(S_2\text{-}Xyl)_2]^{-2}$, $[Fe(SPh)_4]^{-1}$, $[Fe(SPh)_4]^{-2}$. The pre-edge feature for the reduced complexes fall under the rising edge feature.

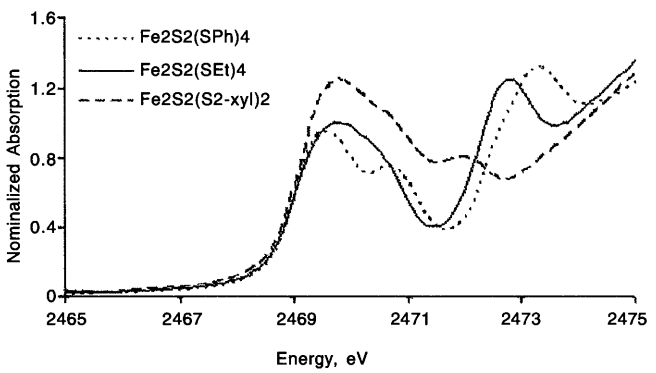

Fig. 12 (a) S K-edge spectra of the fully oxidized 2Fe-2S model complexes: $[Me_2NCH_2Ph]\,[Fe_2S_2(SEt)_4]$ (—), $[Et_4N]_2[Fe_2S_2(S_2\text{-}o\text{-}xyl)_2]$ (---), and $[Et_4N]_2[Fe_2S_2(SPh)_4]$ (...).

between two iron centres and two thiolates to each Fe centres (Fig. 1). The S K-edge XAS spectra of some model complexes: $[Me_3NCH_2Ph]_2[Fe_2S_2(SEt)_4]$, $[Et_4N]_2[Fe_2S_2(SPh)_4]$, $[Et_4N]_2[Fe_2S_2(S2\text{-}o\text{-}xyl)_2]$, $[Et_4N]_2[Fe_2Se_2(SPh)_4]$, $[Et_4N]_2[Fe_2S_2Cl_4]$ and $CsFeS_2$ are shown in Fig. 12. The pre-edge feature occurs between 2468.0 to 2472.0 eV and the edge occurs between 2472 and 2474 eV depending on the nature of the thiolate. The data clearly showed two distinct peaks. It is apparent that the two contributions derive from the two types of sulfur, the μ_2 sulfide and the thiolate. The lower energy contribution was assigned to sulfide as it is more electron rich than the thiolate. This was experimentally confirmed by comparing the S K-edge XAS of $[Et_4N]_2[Fe_2S_2Cl_4]$ and $[Et_4N]_2[Fe_2Se_2(SPh)_4]$ (Fig. 13). The model compound $[Et_4N]_2[Fe_2S_2Cl_4]$ has contributions from the μ_2 bridging sulfide only and $[Et_4N]_2[Fe_2Se_2(SPh)_4]$ has contribution only from

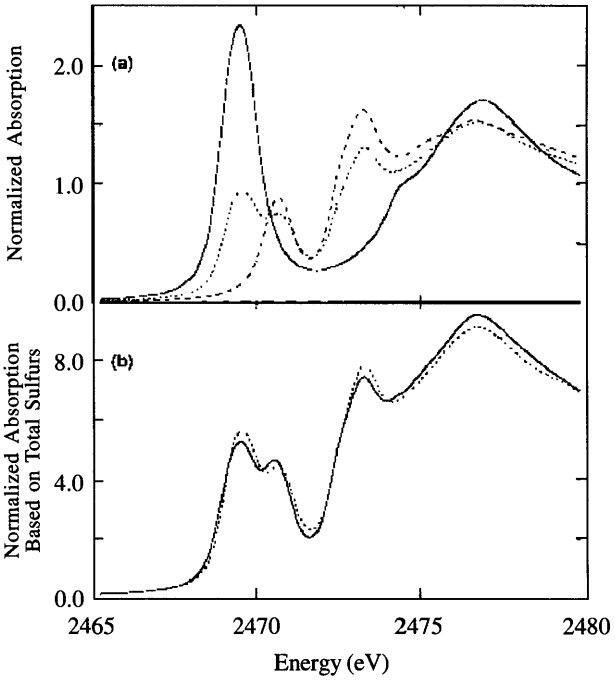

Fig, 13 (a) Normalized S K-edge spectra of $[Et_4N]_2[Fe_2S_2Cl_4]$ (—), $[Et_4N]_2[Fe_2Se_2(SPh)_4]$ (—), and $[Et_4N]_2[Fe_2S_2(SPh)_4]$ (...). Note that the thiolate and sulfide pre-edge peaks are distinguishable in $[Et_4N]_2[Fe_2S_2(SPh)_4]$. (b) Addition of S K-edge spectra of $[Et_4N]_2[Fe_2S_2Cl_4]$ and $[Et_4N]_2[Fe_2Se_2(SPh)_4]$ (s) and comparison to that of $[Et_4N]_2[Fe_2S_2(SPh)_4]$ (—). The solid line was obtained by adding 2/1 of the S K-edge spectrum of $[Et_4N]_2[Fe_2S_2Cl_4]$ and 4/1 of the S K-edge spectrum of $[Et_4N]_2[Fe_2Se_2(SPh)_4]$.

thiolate. A renormalized superposition of these two spectra reproduced the spectra of $[Et_4N]_2[Fe_2S_2(SPh)_4]$. The feature at 2469.6 eV was assigned to a μ_2 bridging sulfide 1s→3d transition and the feature at 2470.8 eVwas assigned to a thiolate 1s→3d transition. The difference in effective nuclear charges of the thiolate and the sulfide is large enough for a clear resolution of the spectra. The covalency values obtained show that oxidized sites are very covalent. The individual contributions of the two components show that the covalency of the μ_2 sulfide is three times more than that of thiolate (Table I). This reflects the enhanced donor capacity of the sulfide due to its greater charge density allowing it to be a better e(π) donor. The spectrum for a reduced binuclear site could not be obtained for a model compound but the reduced spectra was obtained for protein active sites for Rieske[72] and Spinach ferredoxin[74]. Analysis of the reduced spectra reveals distinct Fe(III) and Fe(II) contributions confirming the valence localized electronic structure of the reduced active site. In case of the

Table I

Intensities and Covalency of S K-Edge Pre-edge Data for Fe–S compounds

compound	sulfide intensity	renorm factor	renorm sulfide intensity	covalency of one sulfide per Fe (%)	thiolate intensity	renorm factor	renorm thiolate intensity	covalency of one thiolate per Fe (%)
$[Fe\ (S_2\text{-o-xyl})_4]^-$					1.15	1	1.15	43 ± 2
$[Fe_2S_2(SPh)_4]^{2-}$	1.05	3	3.15	72 ± 5	0.53	1.5	0.80	30 ± 3
$[Fe_2S_2(S_2\text{-o-xyl})_2]^{2-}$	1.46	3	4.38	100 ± 7	0.58	1.5	0.87	33 ± 2
$[Fe_2S_2(SEt)_4]^{2-}$	1.13	3	3.39	78 ± 7	0.45	1.5	0.67	25 ± 3
$[Fe_2Se_2(SPh)_4]^{2-}$					0.84	1	0.84	31 ± 2
$[Fe_2S_2Cl_4]^{2-}$	2.84	1	2.84	65 ± 5	0.94[b]	1[b]	0.94[b]	13 ± 2[b]
$CsFeS_2$	2.42	1	2.42	52 ± 5				
Rieske, oxidized	0.77	4	3.09	71 ± 7	0.23	4	0.91	34 ± 4
Rieske, reduced	0.36	4	1.45	67 ± 6	0.22	4	0.87	32 ± 3

[b]the terminal ligand in this case is Cl and not a thiolate

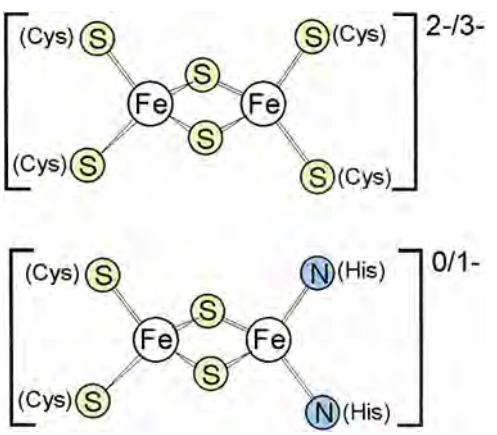

Fig. 14 A normal ferredoxin site (a) and a Rieske centre (b)

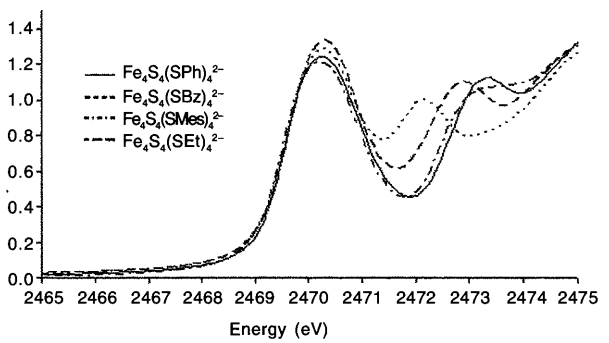

Fig. 15 Normalized S K-edge spectra of tetrameric Fe-S clusters: [*n*-$Bu_4N]_2[Fe_4S_4(SPh)_4]$ (¾), $[Ph_4P]_2[Fe_4S_4(SEt)_4]$ (—), $[Et_4N]_2[Fe_4S_4(Smes)_4]$ (-.-.-.) and $[Et_4N]_2[Fe_4S_4(SBz)_4]$ (...)

Rieske protein, where one of the Fe sites is coordinated by two histidines instead of two cysteines (Fig. 14), the thiolate contribution in the reduced and oxidized site did not change much indicating that the reduction occurs at the site coordinated by two histidines[75].

4.2.3 Delocalized Mixed-Valent Tetramers

The Fe_4-S_4 cluster exists in electron transfer proteins. The biologically active oxidation states are $[Fe_4\text{-}S_4]^{1+}$,$[Fe_4\text{-}S_4]^{2+}$ and $[Fe_4\text{-}S_4]^{3+}$. In Ferredoxins the cluster charge shuffles between $1^+/2^+$ and in High Potential Proteins (HiPiP) the redox couple involves $2^+/3^+$. The resting form in these proteins is the $[Fe_4\text{-}S_4]^{2+}$ state. S-K edge XAS of $[n\text{-}Bu_4N]_2[Fe_4S_4(SPh)_4]$, $[Ph_4P]_2[Fe_4S_4(SEt)_4]$, $[Et_4N]_2[Fe_4S_4(Smes)_4]$ and $[Et_4N]_2[Fe_4S_4(SBz)_4]$ were measured (Fig. 15). The data show intense pre-edge feature around 2469 to 2471 eV. The rising edge position depends on the terminal ligand and follows the same pattern as in the dimeric clusters. The results are shown in Table II.

A direct comparison of the tetranuclear clusters with the binuclear clusters show that the μ_2 sulfide contribution is much larger than that of the μ_3 sulfide contribution in the anti-bonding orbitals normalized per bond. Correspondingly, the terminal ligand contributions increase in the tetranuclear clusters to compensate for the reduced charge transfer from the bridging sulfides. Here too the relative energy positions of sulfide and thiolate pre-edge transitions were measured using the selenide and chloride substituted complexes (Fig. 16) $[Me_4N]_2[Fe_4Se_4(SPh)_4]$ and $[n\text{-}Bu_4N]_2[Fe_4S_4Cl_4]$ where it is found that the sulfide transition again occurs at a lower energy than the thiolate transition but the splitting between the two pre-edge transition energies have decreased compared to the binuclear clusters (Fig. 16a, b).

It is known that the $[Fe_4S_4]^{2+}$ cluster formally contains four $Fe^{2.5}$ ions[76] and can be described as two valence delocalized subdimers , where the extra electron is delocalized on both irons of a sub-cluster,

Table II

Analysis of the S K-edges for Fe-S Clusters

	sulfide		thiolate	
	energy	covalency	energy	covalency
$[Fe_2S_2Cl_4]^{2-}$	2469.5	65		
$[Fe_2Se_2(SPh)_4]^{2-}$			2470.7	25
$[Fe_2S_2(SEt)_4]^{2-}$	2469.6	88	2470.6	30
$[Fe_4S_4Cl_4]^{2-}$	2470.1	39		
$[Fe_4Se_4(SPh)_4]^{2-}$			2470.8	35
$[Fe_4S_4(SEt)_4]^{2-}$	2470.1	39	2740.8	35

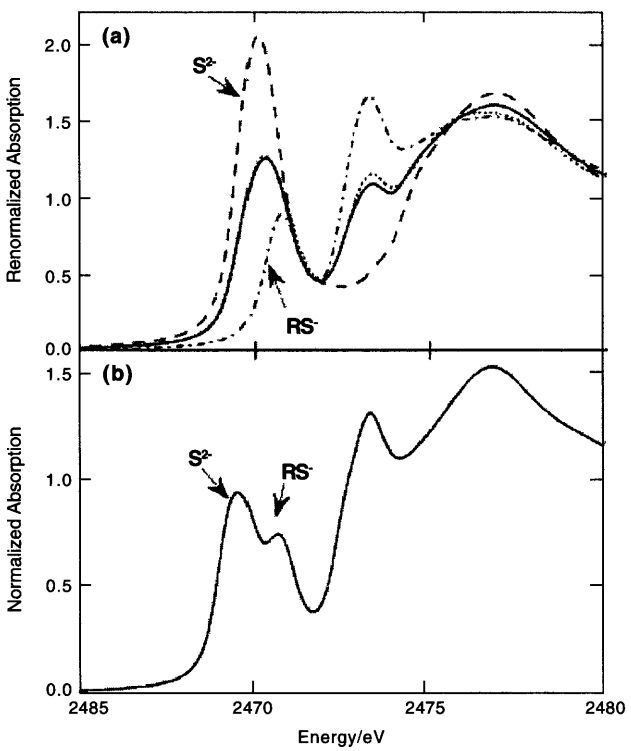

Fig. 16 (a) Normalized S K-edge spectra of $[Me_4N]_2[Fe_4Se_4(SPh)_4]$ (.-.-.-) showing only features due to terminal thiolates, and of $[n\text{-}Bu_4N]_2[Fe_4S_4Cl_4]$ (—) showing only features due to bridging sulfides. The addition of these S K-edge spectra (¾) models well the S K-edge spectrum of $[n\text{-}Bu_4N]_2[Fe_4S_4(SPh)_4]$ (...), containing both the terminal thiolates and the bridging sulfides. The renormalized addition spectrum was obtained by adding 4/8 of the normalized S K-edge spectrum of $[n\text{-}Bu_4N]_2[Fe_4S_4(SPh)_4]$ and 4/8 of the normalized S K-edge spectrum of $[Me_4N]_2[Fe_4Se_4(SPh)_4]$. (b) Normalized S K-edge spectrum of $[Et_4N]_2[Fe_2S_2(SPh)_4]$ demonstrating the decreased energy separation of the pre-edge features of thiolate and sulfide in the 4Fe-4S tetramer as compared to that of the 2Fe-2S dimer

(class III mixed valence), which are in turn antiferromagnetically coupled to give the EPR silent resting form of the cluster. Such an electronic structure is regarded as an outcome of the interplay of Kramer's superexchange[77,78], double-exchange[38-40,79] and vibronic coupling. Super-exchange favours antiferromagnetic coupling, double-exchange leads to delocalization and ferromagnetic coupling, vibronic coupling leads to localization of the extra electron on an iron.

$$E_{\pm}(S_T) = JS_T(S_T+1) + \frac{1}{2}\left(\frac{2}{k_-}\right)x_-^2 \pm \sqrt{\frac{1}{2}\left(\frac{2}{k_-}\right)^2 x_-^2 + B^2\left(S_T+\frac{1}{2}\right)^2} \quad ...(5)$$

The energy of different spin states is given by eq. (5). A relation between experimentally observed covalency from the S K-edge studies and the superexchange coupling constant (J) has been derived[71]. In the same study the double exchange parameter (B)

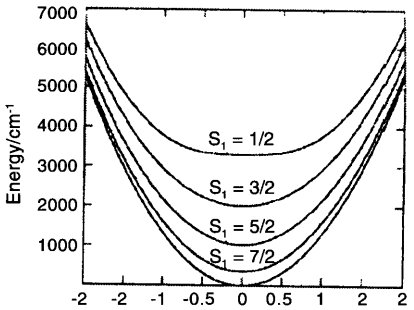

Fig. 17 Energy dependence of the spin-states on *Q*- of the delocalized dimer subsite in the mixed-valence tetra-nuclear Fe-S cluster in the dimensionless antisymmetric breathing mode *x*- calculating using values obtained from experimental results

and vibronic coupling constant (λ^2/k_) have been estimated. Using the experimentally determined parameters, the potential energy surface (Fig. 17) for different possible spin states (using eq. (5), for a Fe_2S_2 sub-cluster, shows that a valence delocalized S = 9/2 electronic configuration is the preferred ground state in the $[Fe_4S_4]^{2+}$ cluster. The higher covalency of the μ_2 sulfide in the dimer as compared to the lower covalency of the μ_3 bridging sulfide in the sub-dimer of the tetramer, leads to a higher super-exchange coupling which opposes double exchange mechanism of electron delocalization forming the valence localized ground state in the dimer described in section *4.2.2.*

4.3 Effect of the Protein on the Electronic Properties of the Cluster

The redox potential of the [Fe-S] clusters vary from -60 to 5 mV for rubredoxins, -180 to -450 mV in $[Fe_2S_2]$ ferredoxins and they vary over a range of 1.0 V in the tetranuclear sites[77]. The redox potential of a protein active site is affected by many environmental factors - hydrogen bonds, effects of C=O amide dipoles, location in the protein and water access. Many theoretical methods have been developed to study the effects of these factors on the electronic structures of the sites[77]. S K-edge XAS has been used to study these effects directly[40,79-81] (Table II). The protein active sites are much less covalent than the corresponding model complexes (Fig. 18 a, b, c). It can be seen that a direct correlation exist between the numbers of H-bonds to the sulfides or thiolates present in the active site and the redox potential and covalency (Table III). The covalency

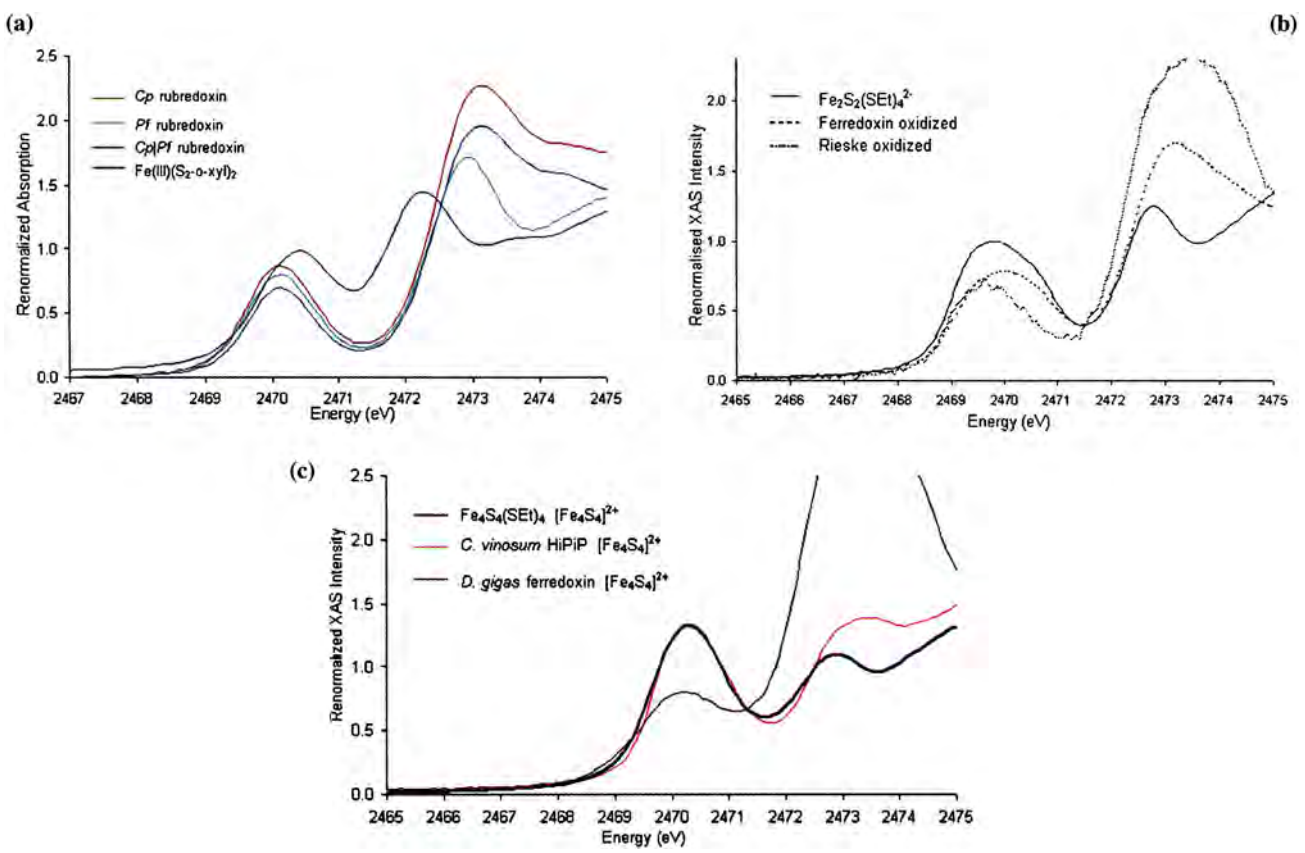

Fig. 18 The experimental spectra of proteins compared to the model complexes. (a) Rubredoxins. (b) Binuclear cluster and (c) Tetranuclear clusters

Table III

Correlation between the numbers of H-bonds to the Sulfides or Thiolates in the Active Site of Fe-S Proteins and the Reduction Potential and Covalency

Protein source	Description of H-Bond						Reduction Poteitial	metal-ligand covalency	
	thiolate			sulfide					
	from	to	Dist.	From	To	Dist	$E_{m,7\ in\ mV}$	sulfide	thiolate
Model complex is $(Et_4N)[Fe(o\text{-}C_6H_4(CH_2S)_2)_2]$ Proc. Nat. Ac. Sci. USA 1975,2868							-1000 mV		38±2
	N Lys6	S Cys5	3.71				-60		
Rubredoxin	N Ile 7	S Cys5	3.60						31±1
Pyrococcus	N Cys 8	S Cys5	3.69						
Furiosus	N Gly 9	S Cys8	3.59						
	N Tyr10	S Cys8	3.51						
Resolution	N Pro 39	S Cys38	3.56						
=0.95 A	N Ile 40	S Cys38	3.53						
	N Cys 41	S Cys38	3.62						
Core $Fe(SR)_4$	N gly 42	S Cys41	3.62						
	N Ala 43	S Cys41	3.62						
The model complex is $(Me_3NCH_2Ph)[Fe_2S_2(SEt)_4]$ J.A.C.S 1983,3905							- 1070 mV	88±5	25±3
	N Cys 47	S Cys 47	3.08						
Ferredoxin	N Ser 46	S Cys 44	3.4						
Spinach	N Gly 42	S Cys 77	3.4	N Ser 38	S1	3.29			
Resolution	N Ser 23	S Cys 39	3.56	N Cys 44	S2	3.09			
= 1.7 A	N Cys 77	S Cys 47	3.52	N Arg 42	S1	3.26	-400	77±4	25±1
Core $Fe_2S_2(SR)_4$	N Ala 41	S Cys 39	3.2						
Rieske from Paracoccus denitrificans							pH=6		
	O Tyr 165	S Cys 139	3.07	N His 161	S1	3.24			
Resolution	N His 141	S Cys 139	3.53	O Ser 163	S1	3.19			
=1.5 A	N Cys 160	S Cys 159	3.83	N Leu 142	S2	3.15	+360	71±8	34±4
Core				N Cys 144	S2	3.6			
$Fe_2S_2(SR)_2(NR)_2$									
The model complex is $(PPh4)_2[Fe_4S_4(SEt)_4]$ J.A.C.S 1983,3905							- 1200 mV	39±2	35±2
Hipip	N 48	SG 46	3.46						
C. Vinosum	N 65	SG 63	3.30						
Resolutio	N 77	SG 77	3.41	N 79	S3	3.42	+365	30±2	35±2
=1.2 A	N 81	SG 46	3.78						
Core $Fe_4S_4(SR)_4$									
FdI D.Gigas Core $Fe_4S_4(SR)_4$	No crystal structure but crystal structure of homologoues show there are eight H-bonds.						-400	23±2	30±2

decreases with increase in H-bonding to the ligating sulfurs. The effective nuclear charge of the H-bonded sulfur increases which decreases its ability to donate electron directly to the metal and results in a more positive redox potential. Furthermore, it is observed that the effects of the H-bonds are more pronounced on the more covalent bridging sulfides than the thiolates in the dimeric clusters as the sulfide covalency decreases more than the thiolate covalency on making the H-bonds to the active site. A linear relation was found between the experimentally measured covalency and the redox potential of the model complexes[74] (Fig. 19). From the plot $1/3^{rd}$ of the observed shift in the redox potential of the protein active site relative to the closest model complex, $Fe_2S_2(SEt)_4$, is due to H-bonds and the rest reflects protein hydrophobic environmental effects. The tetranuclear clusters show two redox couples $1^+/2^+$ as in ferredoxins and $2^+/3^+$ in HiPIPs. HiPIPs, located in the core of the protein, surrounded by hydrophobic residues has five

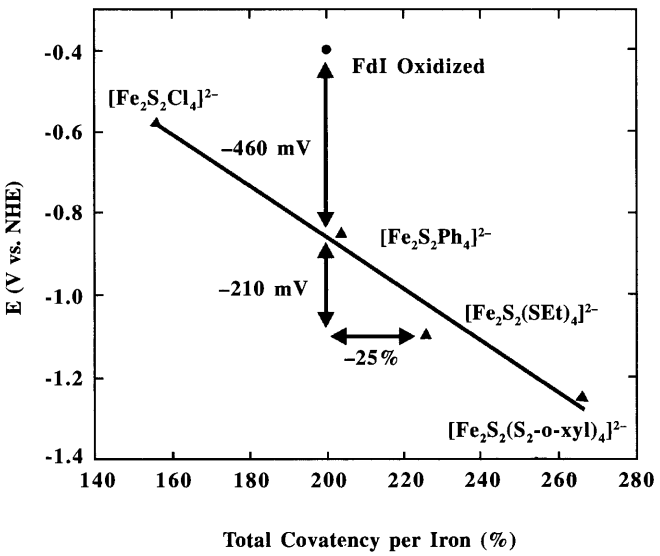

Fig. 19 Correlation between reduction potential and total covalency per iron for a series [2Fe-2S] model compounds with variation in terminal ligation. The variation of solvent used for the different model compounds' studies were taken into account. Dimethylformamide was chosen as the reference solvent and corrected for the variation of the E° of the ferrocene/ferricinium couplein various solvents.

hydrogen bonds and are much more covalent than the ferredoxins which are located on the surface and has eight H-bonds to the cluster ligands. They both in turn are less covalent than the model complex $[Et_4N]_2[Fe_4S_4(SEt)_4]$ [39] (Fig. 18 b) with the effect on Ferredoxin protein being drastic.

Acknowledgements

This work was supported by NSF Grant CHE-9980549 (E. I. S.). We acknowledge invaluable contribution from past graduate and postdoctoral students in the Solomon group and our collaborators on various parts of research presented here.

References

1 J M Nocek, J S Zhou, S DeForest, S Priyadarshay, D N Beratan, J N Onuchic and B M Hoffman, *Chem Rev* **96** (1996) 2459

2 H B Gray and J R Winkler *Annu. rev Biochem* **65** (1996) 537

3 R H Holm, P Kennepohl and E I Solomon *Chem Rev* **96** (1996) 2239

4 S K Chapman, S Daff and A W Munro *Struct Bond* **88** (1997) 39

5 G Palmer *Iron Porphyrins* (Eds. A B P Lever and H B Gray) Addison-Wesley London 1983; **II**, 43

6 M W Makinen and A K Churg, *Iron Porphyrins Physical Bioinorganic Chemistry Series* A B P Lever, H B Gray, (Eds. Addison-Wesley London 1983 Vol. I, p 141.

7 P G Debrunner, *Iron Porphyrins* A B P Lever, H B Gray, Eds. VCH New York, 1989 III, p 137

8 L J Marnett and T A Kennedy, *Cytochrome P450: Structure, Mechanism and Biochemistry*; 2 ed. Ortiz de Montellano (Ed. P R) Plenum New York (1995) p 49

9 A X Trautwein, E Bill, E L Bominaar and H Winkler *Struct Bond* **78** (1991) 1

10 G Loew *Inorganic Electronic Structure and Spectroscopy* E I Solomon, A B P Lever, (Eds. Wiley) New York **II** (1999) p 451

11 E I Solomon and M D Lowery *Science* **259** (1993) 1575

12 E I Solomon, K W Penfield, A A Gewirth, M D Lowery, S E Shadle, J A Guckert and L B LaCroix *Inorg Chim Acta* **243** (1996) 67

13 E T Adman *Advances in Protein Chemistry* C B Anfinsen, F M Richards, J T Edsall and D S Eisenberg (Eds. Academic Press) San Diego **42** (1991) p 145

14 A Messerschmidt *Struct Bond* **90** (1998) 37

15 E N Baker, *Encyclopedia of Inorganic Chemistry* R B King, (Ed. Wiley) Chichester **883** (1994)

16 J M Guss, H D Bartunik, H C Freeman *Acta Crystallog* **B 48** (1992) 790

17 E I Solomon, J W Hare and H B Gray *Proc Natl Acad Sci USA* **73** (1976) 1389

18 B G Malmström, and T J Vänngård *Mol Biol* **2** (1960) 118

19 V T Aikazyan and R M Nalbandyan *FEBS Lett* **55** (1975) 272

20 T Sakurai, H Okamoto, K Kawahara and A Nakahara, *FEBS Lett* **147** (1982) 220.

21 J Peisach, W G Levine and W E Blumberg *J Biol Chem* **242** (1967) 2847

22 B G Malmström, B Reinhammer and T Vänngård *Biochim Biophysc Acta* **205** (1970) 48

23 P J Hart, A M Nersissian, R G Herrmann, R M Nalbandyan, J S Valentine and D Eisenberg *Protein Sci* **5** (1996) 2175

24 L B LaCroix, D W Randall, A M Nersissian, C W G Hoitink, G W Canters, J S Valentine and E I Solomon *J Am Chem Soc* **120** (1998) 9621

25 H Beinert, *Eur J Biochem* **245** (1997) 521

26 N J Blackburn, M E Barr, W H Woodruff and J Oost, S D Vries *Biochemistry* **33** (1994) 10401

27 N J Blackburn, S D Vries, M E Barr, R P Houser, W B Tolman, D Sanders and J A Fee *J Am Chem Soc* **119** (1997) 6135

28 T Tsukihara, H Aoyama, E Yamashita, T Tomizaki, H Yamaguchi, K Shinazwaitoh, R Nakashima, R Yaono and S Yoshikawa *Science* **262** (1996) 1136

29 S Itawa, C Ostermeier and B Ludwig *Nature* **376** (1995) 660

30 C Ostermeier, A Harrenga, U Ermler and H Michel *Proc Natl Acad Sci USA* **94** (1997) 10547

31 P A Williams, N J Blackburn, D Sanders, H Bellamy, E A Stura, J A Fee and D E McRee *Nat Struct Biol* **6** (1999) 509

32 P M H Kroneck, W E Antholine, D H W Kastrau, G Buse, G C M Steffens and W G Zumft *FEBS Lett* **268** (1990) 274

33 D R Gamelin, D W Randall, M T Hay, R P Houser, T C Mulder, G W Canters, S D Vries, W B Tolman, Y Lu and E I Solomon *J Am Chem Soc* **120** (1998) 5264

34 S D George, M Metz, R K Szilagyi, H Wang, S P Crammer, Y Lu, W B Tolman, B Hedman, K O Hodgson and E I Solomon *J Am Chem Soc* **123** (2001) 5757

35 W Lovenberg *Iron Sulfur Proteins* Academic Press New York 1977; Vol. I-III

36 T G Spiro *Iron Sulfur Proteins, Metal Ions in Biology* Wiley New York (1982)

37 R Cammack and T G Spiro (Eds) *Iron Sulfur Proteins, Advances in Inorganic Chemistry* Academic Press San Diego **47** (1999)

38 L Noodleman and E J Barends *J Am Chem Soc* **106** (1984) 2316

39 G Blondin and J J Girerd *Chem Rev* **90** (1990) 1359

40 V Papaefthymiou, J J Girerd, I Moura, J J G Moura and E Munck *J Am Chem Soc* **109** (1987) 4703

41 E L Bominaar, Z G Hu, E Munck, J J Girerd and S A Borsch, *J Am Chem Soc* **177** (1995) 6976

42 I Bertini, G Gori-savellini and C Luchinat *J Biol Inorg Chem* **2** (1997) 114

43 R A Markus and N Sutin *Biochim Biophys Acta* **811** (1985) 265

44 B Hedman, K O Hodgson and E I Solomon *J Am Chem Soc* **112** (1990) 1643

45 S E Shadle, J E Pennerhahn, H J Schugar, B Hedman, K O Hodgson and E I Solomon *J Am Chem Soc* **115** (1993) 767

46 S J George, M D Lowery, E I Solomon and S P Cramer *J Am Chem Soc* **115** (1993) 2968

47 J A Guckert, M D Lowery and E I Solomon *J Am Chem Soc* **117** (1995) 2817

48 L B LaCroix, S E Shadle, Y N Wang, B A Averill, B Hedman, K O Hodgson and E I Solomon *J Am Chem Soc* **117** (1996) 7755

49 J Han, T M Loehr, Y Lu, J S Valentine, B A Averill and J Sanders-Loehr *J Am Chem Soc* **115** (1993) 4256

50 R L Leiberman, D M Arciero, A B Hooper and A C Rosenzweig *Biochemistry* **40** (2001) 5674

51 M Whittekar, D Bergmann, D M Arciero and A B Hooper, *Biochim Biophys Acta* **1459** (2000) 346

52 N Kitajima, K Fujisawa and Y Moro-oka *J Am Chem Soc* **112** (1990) 3210

53 N Kitajima, K Fujisawa, M Tanaka and Y Moro-oka *J Am Chem Soc* **115** (1992) 9232

54 N Kitajima *Adv Inorg Chem* **122** (1992) 11620

55 D W Randall, D R Gamelin, L B LaCroix and E I Solomon *J Biol Inorg Chem* **5** (2000) 16

56 L Basumallick, S D George, D W Randall, B Hedman, K O Hodgson, K Fujisawa and E I Solomon *Inorg Chimica Acta (Special Weighardt Issue)* **337** (2002) 357

57 B E Ramirez, B G Malmström, J R Winkler and H B Gray *Proc Natl Acad Sci USA* **92** (1995) 11949

58 S M Ferguson and G T Babcock *Chem Rev* **96** (1996) 2889

59 P M H Kroneck, W E Antholine, J Reister and W G Zumft, *FEBS Lett.* 242 (1988) 70

60 P M H Kroneck, W E Antholine, J Reister and W G Zumft, *FEBS Lett.* **248** (1989) 212

61 R P Houser, V G Young and W B Tolman *J Am Chem Soc* **118** (1996) 2101

62 E I Solomon, D W Randall and T Glaser *Coord Chem Rev* **200-202** (2000) 595

63 H Robinson, M C Ang, Y G Gao, M T Hay, Y Lu and A H J Wang *Biochemistry* **38** (1999) 5677

64 F Neese, R Kappl, W G Zumft, J Huttermann and P M H Kroneck *J Biol Inorg Chem* **3** (1998) 53

65 R J Gubrial, Y C Fann, K K Surerus, M W Werst, S M Musser, P E Doan, S I Chan, J A Fee and B M Hoffman *J Am Chem Soc* **115** (1993) 10888

66 J N Beratan, J N Betts and J N Onuchic *Science* **252** (1991) 1285

67 S I Chan and P M Li *Biochemistry* **29** (1990) 1

68 T Glaser, B Hedman, K O Hodgson and E I Solomon *Acc Chem Res* **33** (2000) 859

69 F Neese, B Hedman, K O Hodgson and E I Solomon *Inorg Chem* **38** (1999) 4854

70 K W Rose, B Hedman, K O Hodgson and E I Solomon *Inorg Chim Acta* **263** (1997) 315

71 T Glaser, K W Rose, S Shadle, B Hedman, K O Hodgson and E I Solomon *J Am Chem Soc* **123** (2001) 442

72 K W Rose, S Shadle, T Glaser, S deVries, A Cherepanov, G W Canters, B Hedman, K O Hodgson and E I Solomon *J Am Chem Soc* **121** (1999) 2353

73 P Kennepohl and E I Solomon *Inorg Chem* 2002

74 E A Mallart, T Glaser, P Frank, A Aliverti, G Zanetti, B Hedman, K O Hodgson and E I Solomon *J Am Chem Soc* **123** (2001) 5444

75 J Fee, K L Findling, T Yoshida, R Hille, G E Tarr, D Hearshen, W R Dunham, E P Day, T A Kent E Munk *J Biol Chem* **259** (1984) 124

76 H Beinert, R H Holm and E Munck, *Science* **277** (1997) 653

77 A Kramer *Physica* **1** (1934) 191

78 C Zener *Phys Rev* **82** (1951) 403

79 J J Girerd *J Chem Phys* **79** (1973) 1766

80 E I Solomon *Comment Inorg Chem* **3** (1984) 227

81 K W Rose, S E Shadle, M K Eidsness, M K Donald, R A Scott, B Hedman, K O Hodgson and E I Solomon *J Am Chem Soc* **120** (1998) 10743